ELSEVIER

Journal of Fluids and Structures 20 (2005) 359–372

JOURNAL OF FLUIDS AND STRUCTURES

www.elsevier.nl/locate/jnlabr/yjfls

A hydroplastic analysis of a free–free beam floating on water subjected to an underwater bubble

Z. Zong*

Department of Naval Architecture, Dalian University of Technology, Dalian 116024, China

Received 4 March 2002; accepted 8 August 2004

Abstract

Dynamic plastic response of a free–free beam floating on water subjected to an underwater explosion bubble is studied in this paper. A detailed fluid–structure analysis is presented to find the fluid force acting on the beam. Assuming the beam is made from rigid, perfectly plastic material, we obtain the hydroplastic equations governing the dynamic plastic deflection of such a beam. The equations can be easily solved using the Runge–Kutta method. Examples are given to discuss the features of the dynamic plastic response. It is observed that longer beams sustain larger plastic deformations than shorter beams, but shorter beams undergo larger rigid-body motion than longer beams.

© 2004 Elsevier Ltd. All rights reserved.

1. Introduction

Fluid–structure interaction has always been an important part for ship structural analysis. The significant fluid–structure effect on ship dynamics was first realized about 70 years ago when Lewis (1929) successfully explained the big differences in natural frequencies obtained from live tests and predicted from a dry hull model. Since then, fluid–structure interaction has played an important role in prediction of ship hull vibrations (Lamb, 1932; Landweber, 1967; Vorus and Hylarides, 1981; Daidola, 1984), ship dynamic deformations in waves (Aksu and Temarel, 1991; Wu and Moan, 1996; Xia and Wang, 1997; Hermundstad et al., 1999) and ship slamming (Korobkin, 1996; Faltinsen, 1997). As the name suggests, hydroelasticity is the right theory to describe these interactions. Hydroelasticity is currently an active research field, and the latest development may be found in the recent special issue of Journal of Fluids and Structures on marine hydroelasticity (Eatock and Ohkusu, 2000).

Another important fluid–structure interaction effect is dynamic response of a ship hull girder to underwater explosion. An explosion is a chemical reaction in a substance that converts the original explosive material into a gas at very high temperature and pressure. The reacted gas sphere interacts with the surrounding fluid in two different phases. The first is a transient shock wave, which causes a rapid rise in the fluid velocity, and large inertial loading. The peak pressure of this phase is very high (of the order of 10^8 Pa), but its duration is extremely short (of the order of millisecond). The second phase in the explosion is a radial pulsation of the gas sphere. The water in the immediate region of the gas sphere, or ''gas bubble'' as it is usually called, has a large outward velocity and the diameter of the

*Tel.: +86 411 847 07694; fax: +86 411 847 07337.
E-mail address: zongzhi@dlut.edu.cn (Z. Zong).

0889-9746/$ - see front matter © 2004 Elsevier Ltd. All rights reserved.
doi:10.1016/j.jfluidstructs.2004.08.003

bubble increases rapidly. The expansion continues for a relatively long time, the internal gas pressure decreases gradually, but the motion persists because of the inertia of the outward flowing water. The gas pressure at later times falls below the equilibrium value determined by atmospheric plus hydrostatic pressures. The pressure defect brings the outward flow to a stop, and the boundary of the bubble begins to contract at an increasing rate. The inward motion continues until the inside compressed gas acts as a powerful check (stopper) to reverse the motion abruptly. The inertia of the water together with the elastic properties of the gas and water provide the necessary conditions for an oscillating system, and the bubble does in fact undergo repeated cycles of expansion and contraction. In reality, oscillations of a physical bubble can persist for a number of cycles, ten or more such oscillations having been detected in some cases. Compared with the shock wave in the first phase, this phase is characterized by lower peak pressure (about 10–20 percent of that of the shock wave) and much longer duration (about 100–1000 times of that of shock wave). In an underwater explosion, we must consider these two types of loads: shock wave and bubble pulse. Because of their quite different time scales, they are usually analysed separately (Cole, 1962).

Although the pressure produced by a shock is very high, shock effects on the global strength of the hull girder are surprisingly small due to their very short duration (Cole, 1962). The shock effects on structures are characterized by local damage like plating dishing. The bubble behind an explosion, however, has great impact on the global strength of the hull girder due to the fact that the pulse duration of an underwater explosion bubble (of the order 0.1 s) is often close to the lower-frequency vibration modes of a typical ship (of the order several Hz to several tens of Hz). Thus, the induced vibration can easily be so severe that the hull girder fails and a plastic hinge is formed at the point of failure as schematically shown in Fig. 1. This type of failure was repeatedly observed during wartime and live tests. Clear and beautiful photographic records can be found in Keil (1961) and Hicks (1986). The present paper is concerned with global strength of a hull girder, and thus the shock effects are not considered herein. We focus on bubble–hull interaction.

There is a hydroelastic theory (Hicks, 1986; Smiljanic et al., 1994) on the elastodynamic responses of a hull girder to an underwater bubble, and commercial software based on the theory is also available (Deruntz, 1989). The cases of most interest, however, are those in which the structure under consideration is stressed beyond its elastic limit and permanent plastic deformation (explosion damage) results, which may become so large that the structure thins to the point of rupture. Explosion damage has been of a major concern in naval engineering since World War I. The present paper aims at developing a model of dynamic plastic response of a hull girder to an underwater bubble. We use a similar word, hydroplastic, to cater for such analysis.

To simplify the problem as much as possible without losing essential features, we consider a uniform beam freely floating on water. A detailed fluid–structure interaction is presented. Based on the assumption that the beam is made from rigid, perfectly plastic material, the hydroplastic equations governing the dynamic plastic response of the beam to an underwater bubble are given. The equations are solved using the fourth-order Runge–Kutta method. The motion of

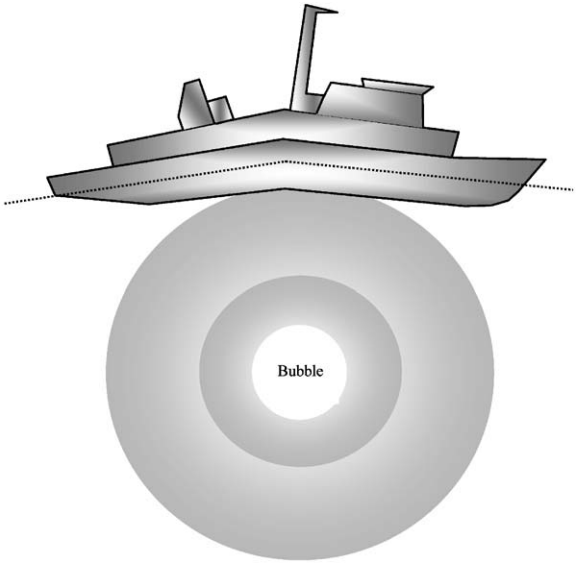

Fig. 1. Plastic deformation of a hull girder under underwater bubble.

the beam is characterized by three phases. The first phase is rigid-body motion while the moment inside the beam builds up. When the moment exceeds the limiting (collapsing) moment of the beam, a plastic hinge is formed and plastic deformation (the second phase) begins. As the bubble loading dies away, plastic deformation ceases after it attains its maximum. A permanent deformation, or damage, is then formed in the structure. Then comes the third phase, that is again rigid-body motion. Dependence of permanent plastic deformation, or damage, on structural geometry and bubble location is investigated through parametric studies. It is concluded from the present study that longer beams suffer larger permanent plastic deformations than shorter beams. The analysis provides a reference for explosion-proofing design.

2. Problem formulation and solution

To facilitate the derivations, we first consider a uniform free–free beam of circular section subjected to a pulsating gas bubble as shown in Fig. 2. We will see later that the assumption of a circular section can be easily removed. Suppose the radius of the beam is R_c. The limiting moment of the beam section is M_0. The beam length is $2L$ with free–free supports at both ends. Two coordinate systems $Oxyz$ and $Ox'y'z'$ are used as shown in Fig. 3, with the origin of the former located at the beam centre and the origin of the latter located at the bubble centre. Note that axes x and $x'$are parallel to the axis of the beam, positive in the bow direction. The deflection of the beam, including rigid-body motion and plastic deformation, is described by $w(x,t)$, and the fluid force acting on the beam per unit length is $f(x,t)$. It is our purpose in the next sections to find both $f(x,t)$ and $w(x,t)$.

It is first assumed that the fluid is inviscid and incompressible. Then there exists a potential Φ satisfying the Laplace equation. It is further assumed that the beam radius is much smaller than the distance from the bubble centre to the beam centre (the stand-off distance). That is, $R_0/R_1 \ll 1$, where R_1 is the stand-off distance. Hence the fluid domain is decomposed into two subdomains: one is D_b near the bubble, and far away from the beam, and the other is D_p near the beam and far away from the bubble. We may write $\Phi = \varphi_b + \varphi_p$, where φ_b denotes the potential purely produced by the bubble, and φ_p denotes all other effects due to the presence of the beam. The main disturbance in the fluid is produced by the bubble, from which comes our third assumption: in D_b: φ_b is much greater than φ_p, i.e., $\varphi_b \gg \varphi_p$, and in D_p, $\varphi_b$is of same order as φ_p, i.e., $\mathcal{O}(\varphi_b) = \mathcal{O}(\varphi_p)$. The solution to Φ can then be found through solving for the two potentials φ_b and φ_p. This method is somewhat like the matched asymptotic expansion method in asymptotic analysis. The fourth assumption is that the beam is slender, i.e., $\varepsilon = R_c/L \ll 1$. By using the fourth assumption, a three-dimensional flow is locally approximated by a two-dimensional flow.

2.1. Bubble dynamics (in D_b)

In the domain D_b, consider an underwater gas bubble, whose radius and pressure at any time are $\varsigma(t)$ and $P(t)$. The initial radius $\varsigma_0$and pressure P_0 are supposed given. They are determined by the parameters of the explosion. In this domain, $\Phi \approx \varphi_b(x', y', z'; t)$ from our third assumption, and φ_b satisfies Laplace equation and the boundary conditions on the bubble surface

$$\nabla^2 \varphi_b = \frac{\partial^2 \varphi_b}{\partial x'^2} + \frac{\partial^2 \varphi_b}{\partial y'^2} + \frac{\partial^2 \varphi_b}{\partial z'^2} = 0, \tag{1}$$

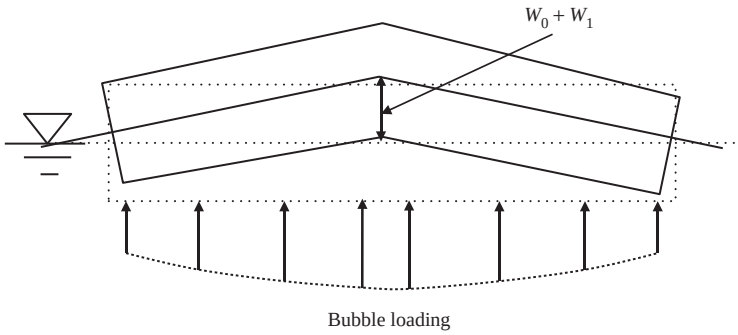

Fig. 2. Simplified beam model.

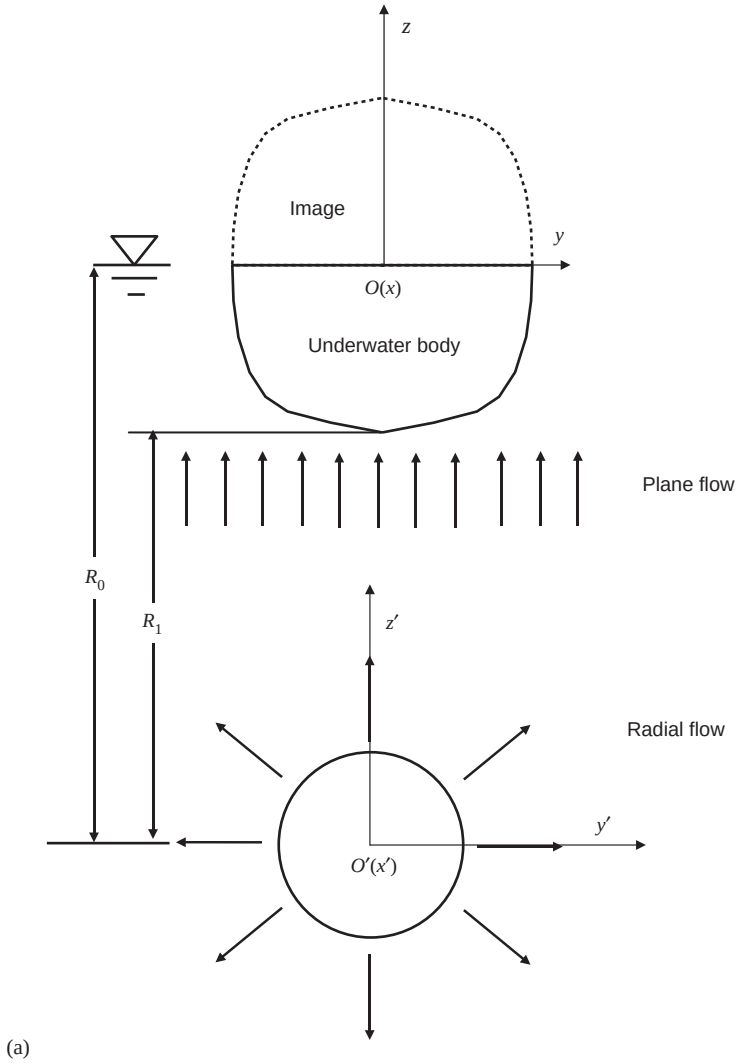

Fig. 3. Decomposition of the flow field into two parts: (a) flow field near the bubble and (b) flow field near the beam.

$$\frac{\partial \varphi_b}{\partial t} = -\frac{P_g}{\rho_0} - \frac{1}{2}|\nabla \varphi_b|^2 + gR_0 \quad \text{at } r' = \varsigma, \tag{2}$$

$$\frac{\mathrm{d}\varsigma}{\mathrm{d}t} = \frac{\partial \varphi_b}{\partial r'} \quad \text{at } r' = \varsigma. \tag{3}$$

On the free surface, the potential should vanish; and at infinity the velocity should also vanish. Thus we have

$$|\nabla \varphi_b| \to 0 \quad \text{at infinity}, \tag{4}$$

$$\varphi_b = 0 \quad \text{at the free surface } (z' = R_0), \tag{5}$$

where P_g is the pressure inside the bubble, R_0 is charge depth (submergence) in absolute value, g is gravity acceleration and ρ_0 is water density. Eq. (5) representing the free surface condition implies that all fluid particles on the free surface have only vertical velocities. It is a high-frequency limit form of the exact free surface conditions (Newman, 1978; Korobkin, 1996).

Inside the bubble, the gas is assumed ideal, and the pressure is uniform. Then we have

$$\frac{P_g}{P_0}=\left(\frac{4/3\pi\varsigma_0^3}{4/3\pi\varsigma^3}\right)^{\gamma}=\left(\frac{\varsigma_0}{\varsigma}\right)^{3\gamma},\quad \gamma=1.4. \tag{6}$$

If the free surface condition (5) is not considered, the solution to Eqs. (1)–(4) is a point source with time-dependent strength $q(t)$ located at the centre of the bubble of the following form:

$$\varphi_b=\frac{q(t)}{r'}. \tag{7}$$

Substituting Eqs. (6) and (7) into Eqs. (2) and (3), we obtain

$$\frac{\mathrm{d}q}{\mathrm{d}t}=-\frac{\varsigma P_0}{\rho_0}\left(\frac{\varsigma_0}{\varsigma}\right)^{3\gamma}-\frac{q^2}{2\varsigma^2}+g\varsigma R_0, \tag{8}$$

$$\frac{\mathrm{d}\varsigma}{\mathrm{d}t}=-\frac{q}{\varsigma^2}, \tag{9}$$

$$q(t)=-\zeta^2\dot{\zeta}. \tag{10}$$

Eqs. (8) and (9) are nonlinear, and can be numerically integrated using the Runge–Kutta method once the initial conditions are given. Its solutions are two time-dependent functions $q(t)$ and $\zeta(t)$.

To cater for the free-surface effect, we apply the method of images by placing a point sink with same strength $q(t)$ at the image position above the free surface. The potential satisfying Eqs. (1)–(6) is then given by (White, 1979; Newman, 1978)

$$\varphi_b=q(t)\left[\frac{1}{\sqrt{x'^2+y'^2+(z'-R_0)^2}}-\frac{1}{\sqrt{x'^2+y'^2+(z'+R_0)^2}}\right]. \tag{11}$$

2.2. Fluid force on the beam (in D_p)

Introducing the following nondimensional equations in domain D_p,

$$\bar{x}=\frac{x}{L},\quad \bar{y}=\frac{y}{R_c},\quad \bar{z}=\frac{z}{R_c}, \tag{12}$$

we have

$$\frac{\partial\Phi}{\partial x}=\frac{1}{L}\frac{\partial\Phi}{\partial\bar{x}},\quad \frac{\partial\Phi}{\partial y}=\frac{1}{R_c}\frac{\partial\Phi}{\partial\bar{y}},\quad \frac{\partial\Phi}{\partial z}=\frac{1}{R_c}\frac{\partial\Phi}{\partial\bar{z}}. \tag{13}$$

Because $\varepsilon=R_c/L\ll 1$ and the derivatives with respect to the nondimensional quantities are of the same order, the above equations indicate that

$$\frac{\partial\Phi}{\partial x}\ll\left(\frac{\partial\Phi}{\partial y},\frac{\partial\Phi}{\partial z}\right),\quad \frac{\partial^2\Phi}{\partial x^2}\ll\left(\frac{\partial^2\Phi}{\partial y^2},\frac{\partial^2\Phi}{\partial z^2}\right). \tag{14}$$

Thus, in the fluid domain near the beam, the three-dimensional flow is locally approximated by a two-dimensional one, as sketched in Fig. 3. This treatment is in fact similar to the strip method (Newman, 1978). Moreover, from the fourth assumption, we conclude that $(y,z)\ll R_1$ in the domain D_p. Or, equivalently, $(y,z)\ll R_0$. Then $\varphi_b$takes the following asymptotic form in D_p:

$$\varphi_b=\frac{q}{\sqrt{(z+R_0)^2+y^2+x^2}}-\frac{q}{\sqrt{(z-R_0)^2+y^2+x^2}}\approx\frac{q}{\sqrt{R_0^2+x^2}}\left(1-\frac{2zR_0}{R_0^2+x^2}\right), \tag{15a}$$

$$\frac{\partial\varphi_b}{\partial z}\approx-\frac{2qR_0}{(R_0^2+x^2)^{3/2}}=v. \tag{15b}$$

With such approximations, we obtain

$$\nabla^2 \Phi = \frac{\partial^2 \Phi}{\partial y^2} + \frac{\partial^2 \Phi}{\partial z^2} = 0 \quad \text{in } D_p, \tag{16a}$$

$$\frac{\partial \Phi}{\partial r} = \frac{\partial w}{\partial t} \cos\theta \quad \text{at } r = R_c. \tag{16b}$$

$$\frac{\partial \Phi}{\partial r} = 0 \quad \text{at infinity}, \tag{16c}$$

$$\Phi = 0 \quad \text{at the free surface } (z = 0), \tag{16d}$$

where θ is the angle between the normal vector and the horizontal axis. Eq. (16b) is the body surface condition, stating that the normal velocity of a fluid particle on the body surface must be equal to the normal velocity of the body surface. It is also called the impermeability body surface condition (Newman, 1978). To account for the free-surface effect required by Eq. (16d), the method of images is used again. The semi-infinite flow in the presence of the free surface is replaced by an infinite flow in the presence of the underwater body of the beam plus its image body above the free surface, as shown in Fig. 3. Suppose the submergence of the circular beam is its radius, then the equivalent flow in the absence of the free surface is an infinite flow past a circle Newman (1978). Then the free-surface condition is omitted with the understanding that the free-surface effect is replaced by an underwater body plus its image above the water.

Because φ_b is known, the above equations uniquely determine φ_p. We may further write the total potential Φ in the form

$$\Phi = \varphi_b + \varphi_D + \varphi_R,$$

where φ_D is the diffraction flow field induced by the beam free of any deformations, thus satisfying

$$\nabla^2 \varphi_D = 0 \quad \text{in } D_p, \tag{17a}$$

$$\frac{\partial \varphi_D}{\partial r} = \frac{\partial \varphi_b}{\partial t} = -v \cos\theta \quad \text{at } r = R_c. \tag{17b}$$

$$|\nabla \varphi_D| \to 0 \quad \text{at infinity}. \tag{17c}$$

The solution to the above problem is well-known to be of the form

$$\varphi_D = v \frac{R_c^2}{r} \cos\theta. \tag{18}$$

Also, φ_R is the radiation potential produced purely by the deflection of the beam, satisfying

$$\nabla^2 \varphi_R = 0 \quad \text{in } D_p, \tag{19a}$$

$$\frac{\partial \varphi_R}{\partial r} = \frac{\partial w}{\partial t} \cos\theta \quad \text{at } r = R_c, \tag{19b}$$

$$\left|\nabla \varphi_R\right| \to 0 \quad \text{at infinity}. \tag{19c}$$

Similarly, the solution is

$$\varphi_R = -\frac{\partial w(x,t)}{\partial t} \frac{R_c^2}{r} \cos\theta. \tag{20}$$

Because $R_c/R_0 \ll 1$, the linearized Bernoulli's equation $P = -\rho_0 \partial\Phi/\partial t - \rho_0 g w$ is used to find the dynamic pressure on the beam (note that static buoyancy and gravity cancel each other out). The fluid force per unit length is then obtained by integrating pressure P on the beam surface,

$$f(x,t) = \oint_{C(x)} P(x,y,z;t) n_z \, \mathrm{d}l(x) = -\rho_0 \oint_{C(x)} \left[\frac{\partial \varphi_b}{\partial t} + \frac{\partial \varphi_D}{\partial t} + \frac{\partial \varphi_R}{\partial t} + g w\right] n_z \, \mathrm{d}l(x), \tag{21}$$

where $\oint_{C(x)} (\cdot) n_z \, \mathrm{d}l(x)$ is the contour integral at section $C(x)$, and n_z is the z-component of directional cosine of the unit normal of the body surface. Substituting Eqs. (15), (18) and (20) into Eq. (21), we obtain

$$f(x,t) = \pi\rho_0 R_c^2 \dot{v} + \pi\rho_0 R_c^2 \dot{v} - \pi\rho_0 R_c^2 \frac{\partial^2 w}{\partial t^2} - 2\rho_0 R_c g w = 2m_a \dot{v} - m_a \frac{\partial^2 w}{\partial t^2} - bw, \tag{22a}$$

where $m_a = \pi\rho_0 R_c^2$ is the added mass of a circular section in water. The first term on the right-hand side of Eq. (22a) is the bubble-induced force without the diffraction effect being considered. The second term is caused by the diffraction effect. They are identical here. In a general case, however, they are not necessarily identical. The third term is the radiation force caused by the beam motion. The fourth term is the buoyancy change caused by heaving of the beam.

Eq. (22a) can be generalized to beams of any cross-sectional shape if similar procedures as above are followed. After lengthy algebra, we obtain

$$f(x,t) = \rho_0 A_s \dot{v} + m_a \dot{v} - m_a \frac{\partial^2 w}{\partial t^2} + \rho_0 B g w = \frac{h}{2} \dot{v} - m_a \frac{\partial^2 w}{\partial t^2} - bw, \tag{22b}$$

where A_s is the cross-sectional area, B is the width of the beam at the waterline; m_a is still the added mass, which will take on different values for different cross-sectional shapes. For a square cross-section, $m_a = 4.754a^2$, where a is the half-width of the square. For cross-sections of general shape, numerical methods are needed to find the added mass (Daidola, 1984; Newman, 1978). A similar equation was obtained by Hicks (1986) by use of a slightly different approach. When a numerical method is applied, the above-mentioned free surface effect should be properly taken into consideration.

2.3. Fluid–beam interaction equation

Because plastic deformation is much larger than elastic response, it is customary in plastic analysis to neglect elastic deformation (Jones, 1989). Then we suppose the beam is made from a rigid, perfectly plastic material as shown in Fig. 4. The transverse force equilibrium and moment equilibrium equations for a straight beam are

$$\frac{\partial Q}{\partial x} = -f(x,t) + m_0 \frac{\partial^2 w}{\partial t^2} \tag{23}$$

and

$$Q = \frac{\partial M}{\partial x}, \tag{24}$$

where M and Q denote the bending moment and shear force, respectively, and m_0 is the mass density per unit length of the beam. The influence of rotational inertia, gravitational effects and transverse shear effects are neglected, while the strains are assumed to remain small (Jones and Wierzbicki, 1987).

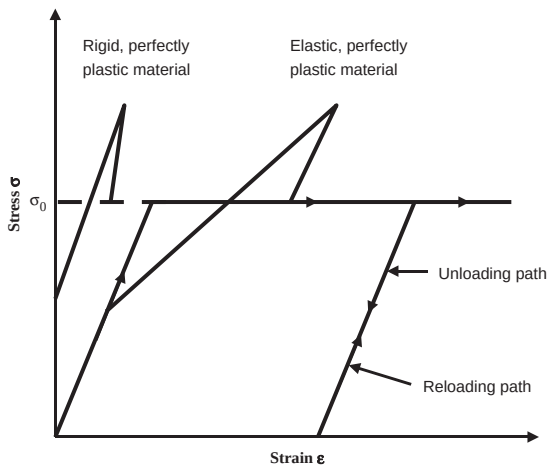

Fig. 4. Elastic, perfectly plastic and rigid, perfectly plastic uniaxial stress–strain idealization.

Substituting Eq. (22b) into Eq. (23) gives

$$\frac{\partial Q}{\partial x} = -h\dot{v} + (m_0 + m_a)\frac{\partial^2 w}{\partial t^2} + bw = g(x)\dot{q}(t) + m\frac{\partial^2 w}{\partial t^2} + bw, \tag{25}$$

where

$$g(x) = \frac{hR_0}{(R_0^2 + x^2)^{3/2}} \quad \text{and} \quad \dot{q}(t) = -\frac{\mathrm{d}}{\mathrm{d}t}(\zeta^2\dot{\zeta}); \tag{26}$$

$m = m_0 + m_a$ is the equivalent mass including hydrodynamic effects. The boundary conditions at the ends $x = -L$ and L of a beam of length $2L$ are

$$Q = 0 \quad \text{and} \quad M = 0. \tag{27}$$

The axial force is zero at the beam end and remains small everywhere else in the beam. Therefore, the present classical beam equations are believed to be valid in the range of moderately large deflection (Jones, 1989).

The beam response is composed of three phases. During the first phase, as the load increases, internal stresses build up in the beam while it is accelerating as a rigid body. Up to the point when the bending moment somewhere in the beam reaches the critical bending moment M_0, a plastic "hinge" forms at the failure point and the second phase of motion begins. During the second phase of motion, plastic deformation accumulates until the point when the plastic deformation rate becomes zero. During the third phase of motion, the bending moment is smaller than the limiting moment, and the plastic deformation rate is zero. The beam that is plastically deformed is either accelerating or decelerating as a rigid body.

2.3.1. *First phase of motion: rigid-body motion*

During the first phase, the beam is accelerating as a rigid body with uniform displacement $w(x, t) = W_0(t)$ governed by the following equation:

$$\frac{\partial^2 M}{\partial x^2} = \frac{\partial Q}{\partial x} = g(x)\dot{q}(t) + m\ddot{W}_0 + bW_0. \tag{28}$$

Integrating the above equation spatially gives

$$\begin{aligned} Q &= \dot{q}(t)\int_{-L}^{x} g(x)\,\mathrm{d}x + (x+L)(m\ddot{W}_0 + bW_0) = \dot{q}(t)\int_{-L}^{x}\frac{hR_0}{(R_0^2+x^2)^{3/2}}\,\mathrm{d}x + (x+L)(m\ddot{W}_0 + bW_0) \\ &= \frac{h\dot{q}(t)}{R_0}\left[\frac{x}{\sqrt{R_0^2+x^2}} + \frac{L}{\sqrt{R_0^2+L^2}}\right] + (x+L)(m\ddot{W}_0 + bW_0). \end{aligned} \tag{29}$$

Setting the shear force to zero ($Q = 0$) at the middle of the beam ($x = 0$), where the bending moment is taken to be a maximum, gives the solution to the rigid body motion, that is,

$$m\ddot{W}_0 + bW_0 = -\frac{h\dot{q}(t)}{R_0\sqrt{R_0^2+L^2}}. \tag{30}$$

Integrating Eq. (29) one more time with respect to x gives

$$\begin{aligned} M &= \frac{h\dot{q}(t)}{R_0}\int_{-L}^{X}\left[\frac{x}{\sqrt{R_0^2+x^2}} + \frac{L}{\sqrt{R_0^2+L^2}}\right]\mathrm{d}x + \frac{1}{2}(x+L)^2(m\ddot{W}_0 + bW_0) \\ &= \frac{h\dot{q}(t)}{R_0}\left[\sqrt{R_0^2+x^2} - \sqrt{R_0^2+L^2} + \frac{L(x+L)}{\sqrt{R_0^2+L^2}}\right] + \frac{1}{2}(x+L)^2(m\ddot{W}_0 + bW_0), \end{aligned} \tag{31}$$

where the boundary conditions were applied. The moment at the mid-span is given from the above equation by setting $x = 0$

$$M' = \frac{h\dot{q}(t)}{R_0}\left[R_0 - \sqrt{R_0^2 + L^2} + \frac{L}{\sqrt{R_0^2 + L^2}}\right] + \frac{1}{2}L^2(m\ddot{W}_0 + bW_0). \tag{32}$$

Introducing Eq. (30) into Eq. (32), we have

$$M' = \frac{h\dot{q}(t)}{R_0}\left[R_0 - \frac{L^2 + 2R_0^2}{2\sqrt{R_0^2 + L^2}}\right]. \tag{33}$$

When $M' > M_0$, a plastic hinge is formed at the middle of the beam.

2.3.2. Second phase of motion: plastic response

The governing equation for plastic deformation is

$$\frac{\partial^2 M}{\partial x^2} = \frac{\partial Q}{\partial x} = g(x)\dot{q}(t) + m\ddot{w} + bw. \tag{34}$$

It is assumed that in addition to the rigid-body motion, there is a relative deformation of the beam expressed as

$$w(x, t) = W_0(t) + W_1(t)X(x), \tag{35}$$

where the amplitude W_0 and W_1 are unknown functions of t and X is a function of x. In view of the symmetric shape of the external dynamic pressure distribution acting on the beam, only the left half-beam is considered. It is assumed that the deformation of the left half-beam is of the form

$$X = \frac{x + L}{L}, \quad -L \leqslant x \leqslant 0. \tag{36}$$

Substituting Eqs. (35) and (36) in Eq. (34), and then integrating spatially gives

$$Q = \frac{h\dot{q}(t)}{R_0}\left[\frac{x}{\sqrt{R_0^2 + L^2}} + \frac{L}{\sqrt{R_0^2 + L^2}}\right] + (x + L)(m\ddot{W}_0 + bW_0) + \frac{(x + L)^2}{2L}(m\ddot{W}_1 + bW_1), \tag{37}$$

$$M = \frac{h\dot{q}(t)}{R_0}\left[\sqrt{R_0^2 + x^2} - \sqrt{R_0^2 + L^2} + \frac{L(x + L)}{\sqrt{R_0^2 + L^2}}\right] + \frac{(x + L)^2}{2}(m\ddot{W}_0 + +bW_0) + \frac{(x + L)^3}{6L}(m\ddot{W}_1 + bW_1). \tag{38}$$

Applying the conditions $M = M_0$ and $Q = 0$ at $x = 0$, we have

$$(m\ddot{W}_0 + bW_0) + \frac{1}{2}(m\ddot{W}_1 + bW)_1 = -\frac{h\dot{q}(t)}{R_0}\frac{1}{\sqrt{R_0^2 + L^2}}, \tag{39a}$$

$$(m\ddot{W}_0 + bW_0) + \frac{1}{3}(m\ddot{W}_1 + bW)_1 = \frac{2M_0}{L^2} - \frac{2h\dot{q}(t)}{L^2}\left[1 - \frac{R_0}{\sqrt{R_0^2 + L^2}}\right]. \tag{39b}$$

Solving the above equations we have

$$m\ddot{W}_0 + bW_0 = \frac{6h\dot{q}(t)}{R_0L^2}\left[-R_0 + \frac{L^2 + 3R_0^2}{3\sqrt{R_0^2 + L^2}}\right] + \frac{6M_0}{L^2}, \tag{40a}$$

$$m\ddot{W}_1 + bW_1 = -\frac{12h\dot{q}(t)}{R_0L^2}\left[-R_0 + \frac{L^2 + 2R_0^2}{2\sqrt{R_0^2 + L^2}}\right] - \frac{12M_0}{L^2}. \tag{40b}$$

The beam reaches its permanent plastic deformation when $\dot{W}_1 = 0$. Note that W_0 in Eq. (40a) accounts for the rigid-body motion at the stage of the second phase of the motion only. To obtain the total rigid-body motion, the final stage of the first phase of motion (displacement and velocity) should be used as initial values for the rigid-body motion at the second stage of motion.

2.3.3. Third phase of motion: rigid-body motion

Plastic deformation ceases but the rigid-body motion continues. Because bubble forces still act on the beam at this stage, the rigid-body motion is an accelerated or decelerated displacement similar to the first phase of motion. The motion at this stage is again described by Eq. (30) with the displacement and velocity at the end of the second stage of motion as initial values.

2.4. The fourth-order Runge–Kutta solution

Eqs. (30) and (40) govern the whole process of the motion. The equations can be analytically solved using the Laplace transform, but the solution is lengthy. We turn to numerical methods, say the fourth-order Runge–Kutta method, which is easy to implement. Let

$$U_1 = t, \quad U_2 = W_0, \quad U_3 = \dot{W}_0 = \dot{U}_2, \quad U_4 = W_1, \quad U_5 = \dot{W}_1 = \dot{U}_4. \tag{41}$$

Then

$$\frac{\mathrm{d}U_1}{\mathrm{d}t} = 1, \quad \frac{\mathrm{d}U_2}{\mathrm{d}t} = U_3, \quad \frac{\mathrm{d}U_3}{\mathrm{d}t} = V_1, \quad \frac{\mathrm{d}U_4}{\mathrm{d}t} = V_2, \quad \frac{\mathrm{d}U_5}{\mathrm{d}t} = V_3, \tag{42}$$

where for the first and third phases (rigid-body motion),

$$V_1 = -\frac{1}{m}\left(\frac{\dot{q}h}{R_0\sqrt{R_0^2 + L^2}} + bU_2\right), \quad V_2 = V_3 = 0; \tag{43}$$

and for the second phase (plastic deformation)

$$V_1 = -\frac{1}{m}\left\{\frac{6\dot{q}h}{R_0L^2}\left[\frac{L^2 + 3R_0^2}{3\sqrt{R_0^2 + L^2}} - R_0\right] + \frac{6M_0}{L^2} - bU_2\right\}, \tag{44a}$$

$$V_2 = U_5, \quad V_3 = -\frac{1}{m}\left\{\frac{12\dot{q}h}{R_0L^2}\left[\frac{L^2 + 2R_0^2}{2\sqrt{R_0^2 + L^2}} - R_0\right] + \frac{12M_0}{L^2} + bU_4\right\}. \tag{44b}$$

Eq. (42) is a set of ordinary differential equations, a form suitable for the Runge–Kutta method. Because it can be found in most of books on numerical analysis, the Runge–Kutta method is not elaborated further in this paper.

3. Numerical results and discussions

As a first example, we consider a bubble of initial radius $\varsigma_0 = 0.75\,\mathrm{m}$ and initial pressure $P_0 = 4.5 \times 10^7\,\mathrm{N/m^2}$; the charge depth is 45 m. The results obtained from Eqs. (7) and (8) are shown in Fig. 5 with solid lines, and the results given by Vermon (1986) are shown with dashed lines. Both are in good agreement.

In the second example, we consider a beam of circular section, whose radius is $R_c = 3\,\mathrm{m}$ and length is $L = 30$, 40 and 50 m, subjected to an explosion bubble with initial radius $\varsigma_0 = 8\,\mathrm{m}$ and initial pressure $P_0 = 1.0 \times 10^5\,\mathrm{N/m^2}$. The submergence of the bubble is $R_0 = 40\,\mathrm{m}$. Material parameters for the beam are: $M_0 = 3.588 \times 10^6\,\mathrm{N\,m}$, $m_a = 28274.3\,\mathrm{kg/m}$, and $A_s = 28.27\,\mathrm{m^2}$.

Fig. 6 shows the time histories of the bubble radius and the force acting on the mid-span of the beam. The bubble radius decreases from its maximum value at the beginning to its minimum value at around $t = 0.4\,\mathrm{s}$. This is the process referred to as "bubble collapse" by some authors. During the process, the bubble radius decreases, but the pressure inside the bubble increases fast. Thus the force acting on the mid-span of the beam increases as the bubble radius decreases. Note that for most of the time while the bubble is collapsing the force is negative, because the bubble

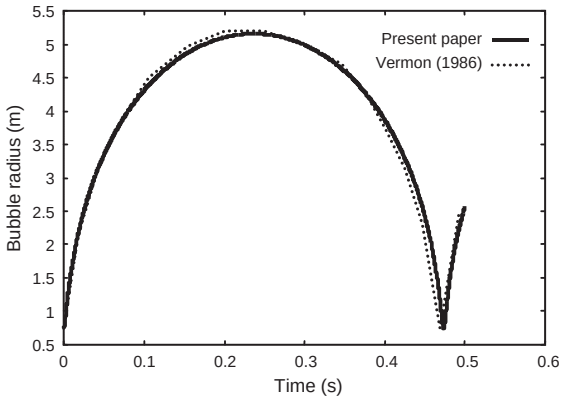

Fig. 5. Comparison of the bubble radius calculated from present paper and Vermon (1986).

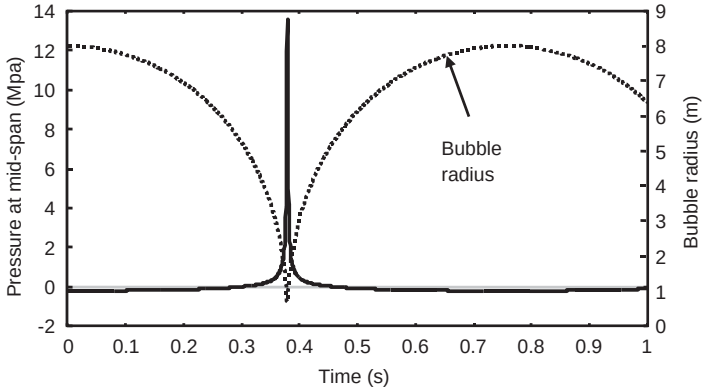

Fig. 6. Time histories of bubble radius and force acting on the mid-span of the beam.

contracts and surrounding water flows towards the bubble. After reaching its minimum radius at around $t = 0.4$ s, the pressure inside the bubble is so large that the bubble "rebounds". The radius then increases with time. During the rebounding process, the force acting on the beam decreases fast to values below zero.

It should be pointed out that Fig. 6 is similar to Fig. 2.1 from Smiljanic et al. (1994). However, in the latter figure $p(t)$ is the pressure inside the bubble but not the hydrodynamic pressure at the ship mid-span as in the present paper. This question is solved by noting that the pressure inside the bubble is the same as that on the interface of the bubble and the immediately surrounding water. Because water is assumed incompressible (all disturbances sweep over the fluid domain immediately) and the bubble is the dominant exciting source, the pressure all over the fluid field would exhibit the same dynamic features of the exciting source (the bubble). Therefore, it is not strange that Fig. 6 is similar to Fig. 2.1 from Smiljanic et al. (1994).

The time history of the rigid-body motion is shown in Fig. 7 (a) and that of the plastic deformation is shown in Fig. 7(b). In terms of the rigid-body motion shown in Fig. 7(a), the beam is first attracted to the bubble. At approximately 0.4 s, the beam suddenly changes its motion direction and moves away from the bubble. Relating this to the bubble motion in Fig. 6, we may obtain an overview of the complete behaviour. As the bubble contracts, the fluid flows toward the bubble, so the beam also moves to the bubble. Meanwhile, the pressure inside the bubble builds up. At around 0.4 s, the pressure inside the bubble is so high that it exerts a large force on the surrounding fluid. The bubble then begins expanding. The fluid transmits a large force to the beam. Under the sudden action of the force, the beam moves from the bubble. The bubble and beam motions are related in the following ways: as the bubble contracts, the beam moves towards to the bubble. As the bubble expands, the beam moves away from it.

In terms of the plastic deformation shown in Fig. 7(b), the beam begins a plastic deformation from $t = 0.4$ s, the time at which the pressure inside the bubble is big. The plastic deformation features a short duration (about 0.2 s) and a sharp rise.

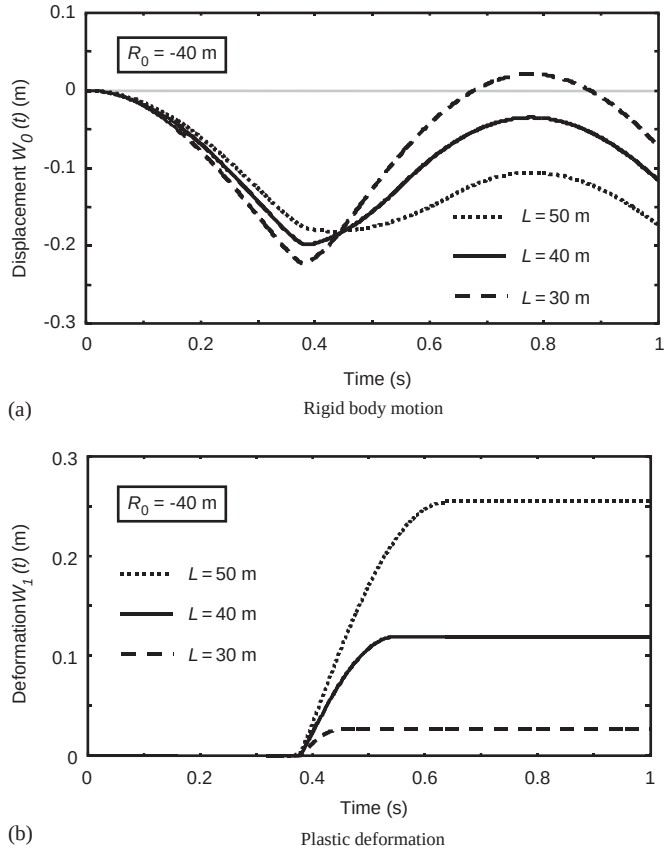

Fig. 7. Time histories of rigid-body displacement and plastic deformation.

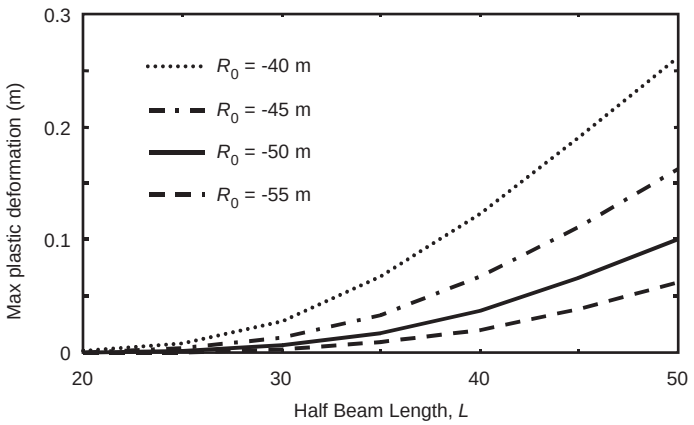

Fig. 8. Dependence of maximum plastic deformation on beam length and bubble submergence.

Fig. 8 shows the dependence of plastic deformation on beam length and bubble submergence. It is interesting to note that shorter beams have smaller plastic deformations than longer beams. This is reasonable if we consider the following two extreme cases. If the beam is infinitely long, only plastic deformation will be induced. If the beam is very small, only rigid-body motion will be produced. As the beam length increases, the beam becomes more vulnerable to plastic deformation.

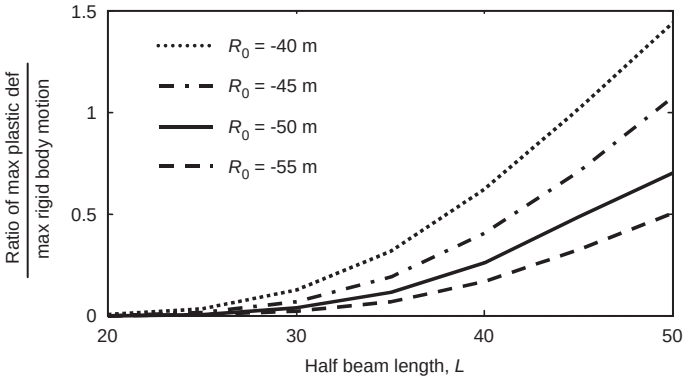

Fig. 9. Ratio of maximum plastic deformation over maximum rigid-body motion.

The above observation can be further clarified by comparing the ratio of maximum plastic deformation over maximum rigid-body motion as shown in Fig. 9. For all the submergences considered here, the above ratio approaches unity as the beam length increases.

The available data on the amount of plastic deformation of a hull girder subjected to an underwater bubble are rare. It seems that only Keil (1961) provided limited information on it. He provided two such cases, in which the amount of the plastic deformation are about 0.15 m and 0.6 m, respectively. The predictions in this paper are within the range.

4. Discussion and conclusions

In this paper, a fluid–structure interaction analysis has been presented leading to the equations governing the dynamic plastic response of a floating free–free beam subjected to an underwater bubble. The solution procedure is characterized by decomposing the physical dynamic process into three phases. In phase I, forces build up in the beam. When the forces in the beam are large enough to exceed the limiting moment of the section, plastic deformation sets in and phase II is initiated. In this phase, both rigid-body motion and plastic deformation are present. When the velocity of plastic deformation is zero, plastic deformation ceases and phase III begins, in which only rigid body motion is considered. Our focus is, however, on phase II to estimate the amount of damage.

Even though the method provided here does not account for the effect of nonuniform cross-sections in the longitudinal direction, the information provided by the method is still useful in the sense (i) that it provides an estimate of the order of the plastic deformation or damage; (ii) that it relates the most dominant factors for the damage; and (iii) that it provides simple benchmark examples for comparison with more complicated numerical methods.

Extension of the method to general cases (such as nonuniform real ship and the asymmetry of the bubble-produced force) is straightforward in terms of the governing equations. But the difficulty lies in the solution, because the prominent difference in a general case is the possible existence of double hinges. Rigid-body motions such as heave and pitch are not difficult to handle because the extensive studies of ship motions in waves over the past four decades have provided a sound solution to the problem. The key step in extending the method is to determine the conditions when a single plastic hinge is formed and when a double hinge is formed.

The most severe assumption is that the radial flow near a bubble is approximated by a planar flow near the beam. The assumption holds true only when the beam is far away from the bubble and the maximum lateral dimensions of the beam are much smaller than the standoff distance. This assumption can be justified if it is compared with the sunlight. The sun is a point source of light if seen from the earth, but the light on the earth can be viewed as a series of plane waves, as we often do in the framework of Newtonian mechanics, due to the fact that the sun is far away from the earth.

Another important approximation is the neglect of the bubble–beam interaction. Only the effect of the bubble on the beam is considered, but the effect of the beam on the bubble is neglected. Again this approximation holds true only if the standoff distance is large. When the bubble is near the structure, their interaction must be considered. It can be expected that in the presence of such interaction, the bubble would no longer be spherical. We argue, however, that the primary effect caused by the bubble is considered in the above model based on multipole expansion of the Laplace equation. The singular solutions to the Laplace equation are of increasing singularity with distance, such as $1/r, (\cos\theta, \sin\theta)/r^2, \ldots$. As the distance r increases, higher-order terms become less and less important, and the dominant contribution comes from the leading order term $1/r$, which is the case treated here.

To remove the above two approximations, a more complicated and computationally intensive fluid–structure interaction model is needed. To the best of our knowledge, such a model is not available yet. We may, however, evaluate the effects of these assumptions on the accuracy of the final results before we go ahead with more complicated computer models.

The effect of the first assumption can be estimated from Eq. (15). The essence of the assumption is to replace the directional cosine by 1 ($\cos\theta \approx 1$). Because in a more accurate model, the factor $\cos\theta$ is always present, the force is expected to be smaller in absolute value than that predicted by the current method. In other words, the current method overestimates the force acting on the beam. Because plastic deformation is caused by the nonuniformity of the force distribution along the beam and rigid-body motion is caused by the force magnitude, it is inferred that introduction of this assumption might overestimate the rigid-body motion, but not necessarily overestimate the plastic deformation.

Let us consider the second assumption. Suppose the influence of the beam on the bubble is not neglected. Then the bubble is no longer spherical. If the bubble is not spherical, a jet directed towards the beam can be formed. This jet can produce a high impact force. So neglecting this jet, or introduction of the assumption that one may ignore the beam effect on the bubble will underestimate the force acting on the beam.

It is expected that this analysis can provide a preliminary prediction of the effect of an underwater bubble on structures, and stimulate more detailed and thorough investigation of the problem.

Acknowledgement

The current work was completed when the author stayed in the Institute of High Performance Computing, Singapore.

References

Aksu, S., Temarel, P., 1991. On the estimation of bending and shear stresses in beamlike ships traveling in a seaway. Philosophical Transactions of the Royal Society of London, Series A—Mathematical Physical and Engineering Sciences 334, 281–292.

Cole, R.H., 1962. Underwater Explosion, second ed. Princeton University Press, Princeton.

Daidola, J.C., 1984. Natural vibrations of beams in a fluid with applications to ships and other marine structures. Transactions of Society of Naval Architects & Marine Engineers 92, 331–351.

Deruntz Jr., J.A., 1989. The underwater shock analysis code and its applications. In Proceedings of 60th Shock and Vibration Symposium (Bethesda), vol. 1, pp. 89–107. Philosophical Transactions of the Royal Society of London, Series A—Mathematical Physical and Engineering Sciences 355, 575–591.

Eatock, T.R., Ohkusu, M., 2000. Special issue on Marine Hydroelasticity—Foreword/editorial. Journal of Fluids and Structures 14, 941–942.

Faltinsen, O.M., 1997. The effect of hydroelasticity on ship slamming. Phil. Trans. R. Soc. A. 355, 1–17.

Hermundstad, O.A., Aarsnes, J.V., Moan, T., 1999. Linear hydroelastic analysis of high-speed catamarans and monohulls. Journal of Ship Research 43, 48–63.

Hicks, A.N., 1986. Explosion induced hull whipping. In: Smith, C.S., Clarke, J.D. (Eds.), Advances in Marine Structures. Elsevier Applied Science Publishers, London, pp. 390–410.

Jones, N., 1989. Structural Impact. Cambridge University Press, Cambridge.

Jones, N., Wierzbicki, T., 1987. Dynamic plastic failure of a free-free beam. International Journal of Impact Engineering 6, 225–240.

Keil, A.H., 1961. The response of ships to underwater explosions. Transactions of Society of Naval Architects and Marine Engineers 69, 366–410.

Korobkin, A., 1996. Water impact problems in ship hydrodynamics. In: Ohkusu, M. (Ed.), Advances in Marine Hydrodynamics. Computational Mechanics Publications, Southampton, pp. 323–367.

Lamb, H., 1932. Hydrodynamics, sixth ed. Dover Publications, New York.

Landweber, L., 1967. Vibration of a flexible cylinder in a fluid. Journal of Ship Research 13, 143–150.

Lewis, F.M., 1929. The inertia of the water surrounding a vibrating ship. Transactions of Society of Naval Architects and Marine Engineers 37, 1–20.

Newman, J.N., 1978. Marine Hydrodynamics. The MIT Press, Cambridge.

Smiljanic, B., Bobanac, N., Senjanovic, I., 1994. Bending moment of ship hull girder caused by pulsating bubble of underwater explosion. In: Faltinsen, O. (Ed.), Proceedings Hydroelasticity in Marine Technology. A.A. Balkema, Trondheim, pp. 149–156.

Vermon, T.A., 1986. Whipping response of ship hulls from underwater explosion bubble loading. Technical Memorandum 86/255, Defence Research Establishment Atlantic, pp. 1–41.

Vorus, W.S., Hylarides, S., 1981. Hydrodynamic added-mass matrix of vibrating ship based on a distribution of hull surface sources. Transactions of Society of Naval Architects and Marine Engineers 89, 397–416.

White, F.M., 1979. Fluid Mechanics. McGraw-Hill Book Company, New York.

Wu, M.K., Moan, T., 1996. Linear and nonlinear hydroelastic analysis of high-speed vessels. Journal of Ship Research 40, 149–163.

Xia, J.Z., Wang, Z.H., 1997. Time-domain hydroelasticity theory of ships responding to waves. Journal of Ship Research 43, 286–300.